

PACS numbers: 42.55.Px; 42.60.Jf
DOI: 10.1070/QE2004v034n03ABEH002628

Use of the Talbot effect for measuring the phase-to-amplitude ratio for a gain grating induced in a flashlamp-pumped Nd : YAG crystal

N.N. Il'ichev, V.V. Tumorin

***Abstract*. Based on the Talbot effect, a method is developed for measuring the phase-to-amplitude ratio for gain gratings in saturated laser media. Experiments performed by this method showed that the gain grating induced in a Nd : YAG crystal is predominantly the amplitude one, with the phase-to-amplitude ratio of no more than 0.3 under our experimental conditions.**

Keywords: *Talbot effect, gain grating, Nd : YAG crystal, degenerate four-wave mixing.*

1. Introduction

Interest in the study of the interaction of light waves on gain gratings has quickened recently due to the development of laser systems with phase conjugation by degenerate four-wave mixing (DFWM) in a saturated laser medium [1 – 4]. An advantage of this phase conjugation method compared to the conventional phase conjugation by stimulated Brillouin scattering is, in particular, the possibility of the development of high-brightness self-starting laser systems [5 – 9]. In such systems, the positive feedback required for the initiation of lasing is produced by recording a volume hologram in saturated gain gratings in the active medium of the laser by means of the self-consistent superluminescence radiation field [10]. To understand processes resulting in the appearance of the positive feedback in these systems, it is important to elucidate the nature of gratings produced in the active medium [11].

Due to a number of reasons, the recording of an amplitude saturated gain grating is accompanied by the production of phase gratings of variations in the refractive index of an amplifying medium. In some cases, the diffraction efficiencies of the phase and amplitude components of the grating being formed can be comparable, which is revealed in the energy and spectraltemporal characteristics of radiation of a laser with the DFWM mirror. The ratio of the diffraction efficiencies of the phase and amplitude components of gain gratings is described by the parameter β, which is equal to the ratio of the real (χ_{re}) and imaginary (χ_{im}) parts of the resonance susceptibility of the laser medium [12]:

$$\beta = \frac{\chi_{re}}{\chi_{im}} = \frac{k\Delta n}{\alpha}, \qquad (1)$$

where k is the wave number; α is the gain of the active medium; Δn is the difference of the refractive indices of the inverted and noninverted laser medium.

The most popular active medium used in solid-state DFWM lasers is a Nd : YAG crystal, which explains particular interest in the study of its nonlinear properties. The authors of Ref. [13] studied theoretically DFWM in the active media of solid-state lasers on a thermal nonlinearity produced by photoinduced heat release. According to Ref. [13], the thermal nonlinearity in a Nd : YAG laser is 4 – 5 orders of magnitude lower than the gain nonlinearity, which is explained by a comparatively large cross section for the stimulated laser transition.

The DFWM process substantially depends on the fine structure of the main 1064-nm $^4F_{3/2} - {}^4I_{11/2}$ line of a Nd^{3+} : YAG laser [14], which makes the gain profile asymmetric. For this reason, the imaginary part of the gain does not vanish at the maximum of the gain line, resulting in the appearance of the phase component of the gain grating with $\beta \approx 0.05$ [15]. It is the presence of the fine structure in the gain line that is responsible for the peculiarities of the self-modulation regime of oscillations in a Nd : YAG ring laser [15, 16].

The phase component of the gain grating can also appear due to the up-conversion population of high-lying metastable levels [$^2(F_2)_{5/2}$, $^4D_{3/2}$, and $^2P_{3/2}$] of the $4f$ shell in the Nd^{3+} ion with high polarisabilities upon multistage excitation by a high-power broadband flashlamp [17, 18]. The interferometric measurements of the electron component of a change in the refractive index [17] of the Nd : YAG crystal produced by flashlamp pumping showed that the refractive index at the 633-nm probe wavelength increased nonlinearly with increasing the gain α. Thus, for $\alpha = 0.45$ cm^{-1}, the parameter β achieved 1.2. It was also found that variations in the refractive index 'follow' variations in the population of the metastable $^4F_{3/2}$ level with the delay time of 1 – 3 μs, which is equal approximately to the lifetime of the metastable $^2(F_2)_{5/2}$ level.

The mechanism of grating production by degenerate and nondegenerate four-wave mixing in a flashlamp-pumped Nd : YAG crystal was studied in Ref. [12]. This study confirmed the fabrication of highly efficient diffraction

N.N. Il'ichev, V.V. Tumorin A.M. Prokhorov General Physics Institute, Russian Academy of Sciences, ul. Vavilova 38, 119991 Moscow, Russia

Received 27 June 2003; revision received 20 October 2003
Kvantovaya Elektronika **34** (3) 283 – 288 (2004)
Translated by M.N. Sapozhnikov

gratings of a variation in the refractive index in the flashlamp-pumped Nd : YAG crystal.

In Ref. [19], the phase component of the gain grating in a Nd : YAG crystal was separated using a Nd : yttrium orthoaluminate laser. It was shown in this paper that, in the case of a substantial gain saturation in the Nd : YAG crystal, the parameter β at 1.079 μm did not exceed 0.2. However, the parameter β in papers [12, 17–19] was determined either by comparing the experimental diffraction efficiency of a DFWM mirror with the calculated values or by studying the refractive-index gratings using probe beams at the nonresonance frequency. As far as we know, no direct measurements of the real and imaginary parts of the resonance susceptibility of the Nd : YAG crystal have been performed so far.

The most clear method for studying the nature of gratings produced in nonlinear optical media is based on the effect of self-reproduction of the radiation field in the near-field zone behind the grating (the Talbot effect [20]). It is this method that was used to demonstrate the phase nature of gratings produced in silicon exposed to radiation from a neodymium laser [21]. The method is based on the fact that, if a plane monochromatic wave is incident on a 'thin' grating with period Λ, then the grating image is reconstructed at distances that are multiples of the Talbot distance $z_T = 2\Lambda^2/\lambda$ behind the grating. The grating image is also reconstructed at distances $(1/2 + m)z_T$, where $m = 0, 1, 2, \ldots$, but in this case the image is transversely shifted by the distance $\Lambda/2$. The contrast of the interference pattern produced by the probe and diffracted beams is a periodic function of the distance z to the grating with period $z_T/2 = \Lambda^2/\lambda$.

In the case of a sinusoidal amplitude grating with a small modulation depth of transmission, the contrast reaches its maxima at distances $m\Lambda^2/\lambda$ from the grating. A sinusoidal phase grating has minima of the contrast at these distances, while the maxima of the contrast are observed at distances $(1/2 + m)\Lambda^2/\lambda$ from the grating. If a grating is a superposition of the phase and amplitude components, the maxima of the contrast will be displaced with respect to the maxima of the contrast for a purely amplitude grating to one or other side depending on the sign of β. We used this method for measuring the parameter β in this paper.

It is difficult to apply this method to standard cylindrical active elements because, on the one hand, the grating should be 'thin', i.e., the reduced length L/n of the active element (where L is the active-element length and n is the refractive index) should be substantially smaller than the characteristic distance $\Lambda^2/(2\pi\lambda)$ at which the contrast of the interference pattern changes, while, on the other hand, the interfering beams of the lth diffraction order should not diverge strongly at the distance Λ^2/λ, i.e., $l\Lambda \ll r$, where r is the active-element radius. These two conditions determine the requirement to the geometrical dimensions of the active element: $r^2 \gg 2l^2 \times \pi\lambda L/n$. This requirement can be somewhat alleviated by considering only the interference of the probe beam and two beams of probe radiation diffracted in the first order from the saturated gain grating, which propagate at angles $\pm\lambda/\Lambda$ to the direction of propagation of the probe beam ($l = -1, 0, 1$). However, even in this case, the contrast of the interference pattern was not reconstructed at a distance of Λ^2/λ from the standard $\varnothing 6.3 \times 60$ mm active element. For this reason, we constructed images of the active-element ends by means of a telescope in our experiments and observed a change in the contrast of the interference pattern both in front of and behind the active-element image.

2. Experimental setup

Figure 1 shows the scheme of the experimental setup. We studied Nd^{3+} : YAG active elements placed inside standard K-301 quantrons. The resonator of a free-running master oscillator was formed by highly reflecting mirror (*1*) and glass etalon (*4*) of thickness 1 cm. The volume of the fundamental mode of the resonator was increased with the help of $4^{\times}$ telescope (*2*). By adjusting the distance between the telescope lenses, the aperture of $\varnothing 6.3 \times 100$-mm active element (*3*) was completely filled with the fundamental mode. The output radiation of the master oscillator was incident on a system of glass wedges (*6*). The inner surfaces of the wedges formed a wedge-like gap with the angle ~ 0.53 mrad of thickness a few tens of micrometres. The interfering beams reflected from these surfaces were incident on $\varnothing 6.3 \times 60$-mm active element (*7*) and recorded in it a saturated gain grating with a step of ~ 1 mm. The probe beam reflected from glass substrate (*5*) with the reflectivity ~ 4 % and from the front surface of a system of wedges (*6*) was incident on active element (*7*) at an angle of ~ 3 mrad to the plane of propagation of saturating beams.

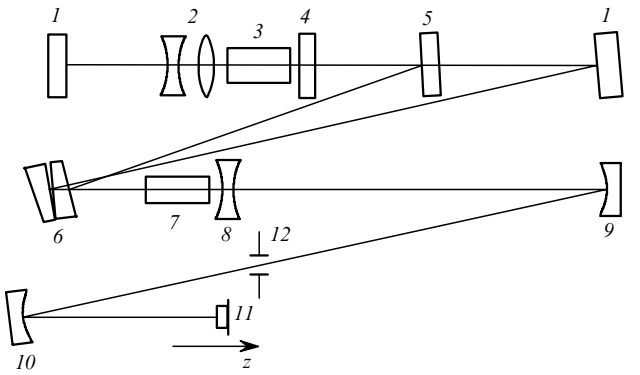

Figure 1. Scheme of the experiment: (*1*) highly reflecting mirror; (*2*) telescope; (*3*) $\varnothing 6.3 \times 100$-mm active element; (*4*) etalon; (*5*) substrate with one AR surface; (*6*) system of wedges; (*7*) $\varnothing 6.3 \times 60$-mm active element; (*8*) compensating negative lens; (*9*) substrate with the radius of curvature of 2 m; (*10*) highly reflecting mirror with the radius of curvature of 1.2 m; (*11*) CCD camera; (*12*) slit.

Therefore, the ratio of the energy densities of the probe and saturating beams averaged over the active-element cross section was ~ 0.02. In this case, the projection of the direction of propagation of the probe beam on the plane of saturating beams coincided with the bisectrix of the angle between saturating beams. The laser system operated at a pulse repetition rate of 2.5 Hz. Negative lens (*8*) with a focal distance of 7.5 m was used to compensate for a thermal lens induced in active element (*7*). A telescope, consisting of substrate (*9*) with a spherical surface with a radius of curvature of 2 m and of highly reflecting mirror (*10*) with a radius of curvature of 1.2 m, imaged active element (*7*) on CCD array (*11*). The output video signal of the CCD array was digitised and recorded in a computer. Variable slit (*12*) located in the focal plane of the telescope was used to filter the side spatial maxima of the higher-order

diffraction of the probe beam from the gain grating. Slit (*12*) also blocked high-power saturating beams.

The power of saturating beams was varied by varying the pump energy of the master oscillator. The lasing threshold was ~ 18 J. The experiments were performed well above the lasing threshold (30–50 J). In this case, the oscillator emitted many spikes in a pulse in the free-running regime, with the train duration of ~ 200 μs and the spikes separated by 1–3 μs. The pump energy of amplifier (*7*) was constant and equal to 50 J. The delay time of pump pulses of amplifier (*7*) upon varying the output energy of the master oscillator was adjusted to achieve the maximum output from amplifier (*7*).

3. Experimental results

Figure 2 shows the dependence of the gain in the energy of saturating beams in active element (*7*) on the radiation energy incident on the amplifier. The energy of saturating beams was varied in experiments between 5 and 16 mJ. Therefore, the saturated energy gain α averaged over the active-element volume was varied between 0.38 and 0.44 cm^{-1}. According to Ref. [17], the refractive index of a Nd : YAG crystal at 633 nm drastically increases at such gains ($k dn/d\alpha \approx 5$). It follows from Ref. [12] that in this case the diffraction efficiency of the phase grating of the refractive index should exceed that of the amplitude saturated gain grating.

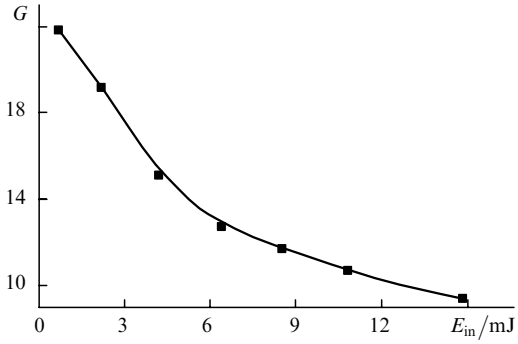

Figure 2. Dependence of the energy gain G in active element (*7*) on the saturation energy E_{in} of beams incident on the amplifier.

The probe beam and beams scattered to the first diffraction order, which propagate from both sides of the probe beam, were separated in experiments by slit (*12*). The interference patterns of these beams were detected with a CCD camera by moving the camera along the z axis in both directions from the image of active element (*7*) (Fig. 3). From the interference patterns obtained this way, the central part of the beam with the most uniform probe-beam intensity distribution was cut so that this part would contain an integer number of periods of the interference pattern. Then, the interference patterns were integrated over the vertical coordinate of the beam. Because the transverse distribution of the probe-beam intensity and the contrast of the interference pattern were inhomogeneous over the beam cross section, the contrast was calculated from the expression

$$K = \pi \frac{\int_{-m\Lambda/2}^{m\Lambda/2} |F_n(x) - f(x)| \mathrm{d}x}{\int_{-m\Lambda/2}^{m\Lambda/2} [F_n(x) + f(x)] \mathrm{d}x}, \qquad (2)$$

where Λ is the step of the interference pattern; m is an integer; $f(x)$ is the experimental distribution of the radiation energy density over the beam cross section along the horizontal coordinate; $F_n(x)$ is the approximation of the function $f(x)$ by a polynomial of degree n. The degree n was chosen so that the function $F_n(x)$ reproduced only the smooth transverse distribution of the energy density of the probe beam but not the modulation of the energy density over the horizontal coordinate caused by the interference of the beams.

This method for contrast measuring is illustrated in Fig. 4 by the functions $f(x)$ and $F_n(x)$, which were obtained after the processing of the interference pattern in Fig. 3a. In this case, the contrast of the interference pattern calculated from (2) was 0.4.

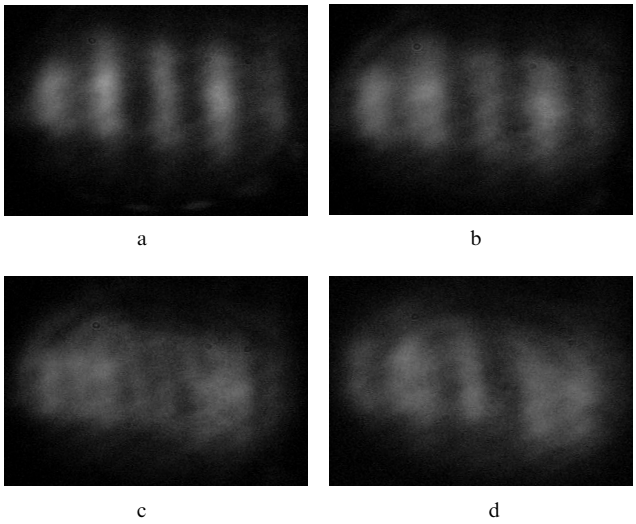

Figure 3. Images of the interference pattern at distances $z = 0$ (a), 20 (b), 40 (c), and 60 cm (d) from the exit end of the active element.

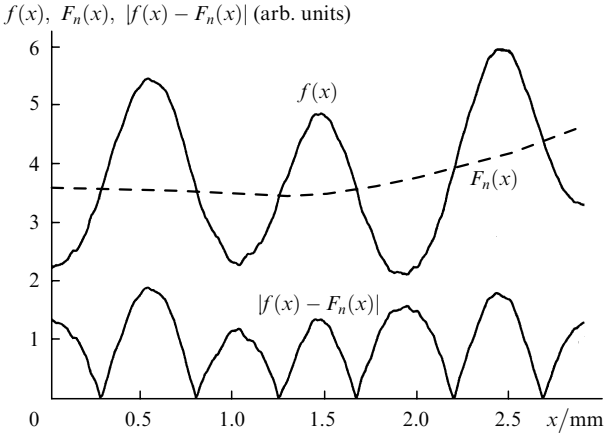

Figure 4. Illustration of the method for determining the contrast of the interference pattern.

The experimental dependence of the contrast K of the interference pattern on the displacement of the CCD array along the z axis is shown by squares in Fig. 5. The distance along the z axis is recalculated for a beam in the object plane of the telescope consisting of mirrors (*9*) and (*10*). The position $z = 0$ corresponds to the central region of active element (*7*).

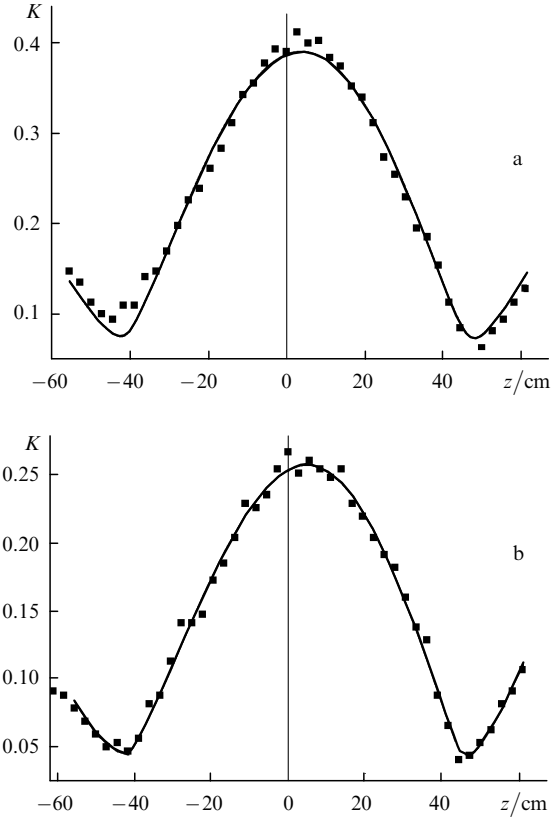

Figure 5. Variation in the interference-pattern contrast along the z axis for the energies of saturating beams equal to 16 (a) and 6 mJ (b). Solid curves are calculations for $\beta = 0.14$ (a) and 0.19 (b).

4. Experimental data processing

We developed a simple one-dimensional mathematical model to interpret our experimental data. The calculations were performed in the approximation of a 'thin' saturated gain grating. In this case, the gain increment γ in the active element was determined from the differential equation

$$T_r \frac{d\gamma(x,t)}{dt} + \gamma = P(t) - (\exp\gamma - 1)I(x,t) \tag{3}$$

with the initial condition

$$\gamma(x,0) = \ln 8,$$

where T_r is the lifetime of the upper laser level; $P(t)$ is the optical pump rate; $I(x, t)$ is the intensity of saturating radiation incident on the amplifier expressed in the units of the saturation intensity. The onset of lasing was observed in experiments when the pump power of the amplifier was approximately maximal and the small-signal gain achieved 8. The time dependence of the pump rate was approximated by the Gaussian $P(t) = P(0)\exp[-(t/T_p)^2]$ for $T_p \approx 60$ μs. The value of $P(0)$ was chosen to provide the maximal small-signal gain equal to 24. The time dependence of the saturating radiation intensity was also approximated by the Gaussian $I(x, t > 0) = I(x)\exp[-(t - t_m)^2/T_s^2]$ for $T_s \approx 80$ μs and $t_m \approx 40$ μs. The transverse distribution of the saturating radiation intensity was specified by the function $I(x) = [4I_s \cos^2(\pi x/\Lambda) + I_{pr}]\exp(-x^2/w^2)$, where I_{pr} and I_s are the maximal in time intensities at the centres of the probe and saturating beams, respectively.

The gain increment found from Eqn (3) was used to describe the field amplitude $A(x, t)$ of the probe beam behind the amplifier:

$$A(x,t) = \sqrt{I_{pr}}\exp\left[\frac{1-i\beta}{2}\gamma(x,t) - \left(\frac{1}{2w^2} + \frac{ik}{2R}\right)x^2 - \frac{(t-t_m)^2}{2T_s^2}\right], \tag{4}$$

where R is the residual radius of curvature of the wave front of radiation behind the compensating lens. By using the Fourier transform, we found the region of the spatial spectrum of probe radiation, which included the three main spatial components of radiation with the maximal intensity

$$F(l,t) = \int_{-r_a}^{r_a} A(x,t)\exp(2\pi i x l/\Lambda)dx, \quad -1.5 < l < 1.5, \tag{5}$$

where r_a is the active element radius. The transverse distribution $A'(x, t, z)$ of the field at the distance z from the active-element image was calculated with the help of the inverse Fourier transform taking into account the phase shift for different spatial components of the field:

$$A'(x,t,z) = (1/\Lambda)\int_{-1.5}^{1.5} F'(l,t,z)\exp(-2\pi i x l/\Lambda)dl, \quad F'(l,t,z) = F(l,t)\exp(i\pi l^2\lambda z/\Lambda^2). \tag{6}$$

The transverse distribution of the radiation energy density in the probe beam at the distance z from the active-element image was found by integrating the radiation intensity in time:

$$W(x,z) = \int_0^\infty |A'(x,t,z)|^2 dt. \tag{7}$$

The distributions obtained this way were processed similarly to the experimental data, and the contrast of the interference pattern was calculated from expression (2). By varying the parameters β, R, Λ, and I_s we fitted the experimental data by the calculated curves of contrast variation along the z axis. Note that, although some of these parameters can be measured directly in experiments with one or other accuracy, the information contained in the curve of contrast variation along the z axis is sufficient for the unique determination of all these parameters. Thus, the step Λ of the grating determines the period of the change in the contrast of the interference pattern along the z axis and can be calculated from the distance between the positions of the contrast minima. The displacement of the maximum of the contrast-variation curve with respect to the active-

element position ($z = 0$) is determined by the parameter β. The contrast at $z = 0$ is determined by the saturating radiation intensity I_s. The residual radius of curvature of the wave front of probe radiation behind compensating lens (*8*) results in the aperiodicity of the contrast-variation function along the z axis.

To describe quantitatively the discrepancy between the experimental and calculated data, we introduce the optimisation parameter

$$Q = \frac{1}{N}\sum_{i=1}^{N}(K_i^{\mathrm{exp}} - K_i^{\mathrm{calc}})^2,$$

where N is the number of experimental points; K_i^{exp} and K_i^{calc} are the experimental and calculated values of the contrast at the same points on the z axis. By varying successively and repeatedly the parameters β, R, Λ, and I_s we found their optimal values at which the minimal optimisation parameter $Q_{\min}$ was achieved. This parameter was comparable with the dispersion of the experimental data caused by an arbitrary choice of the region in the cross section of the probe beam for calculating contrast from (2).

Consider the 'sensitivity' of determining parameter β by the method of least squares to the variation of the parameters R, Λ, and I_s with respect to their optimal values. The dependences of the optimisation parameter Q on the parameter β for several values of R at the energy of saturating beams of 6 mJ and the optimal parameters Λ, and I_s are shown in Fig. 6. For each value of the parameter R, the own minimal parameter $Q_{\min}(R)$ and the corresponding optimal parameter $\beta(R)$ were found. Figure 7 shows the dependence of $Q_{\min}(R)$ on $\beta(R)$ obtained this way, as well as the dependences of $Q_{\min}$ on β obtained by varying the parameters Λ and I_s with respect to their optimal values. One can see that this method for determining parameter β is the most 'sensitive' to variations in the parameter R. For example, in the case presented in Fig. 6, the neglect of the residual radius of curvature of the wave front of probe radiation ($1/R = 0$) considerably reduces the parameter β down to 0.1, while the necessity to determine the parameters β and R simultaneously reduces the accuracy of this method approximately by half.

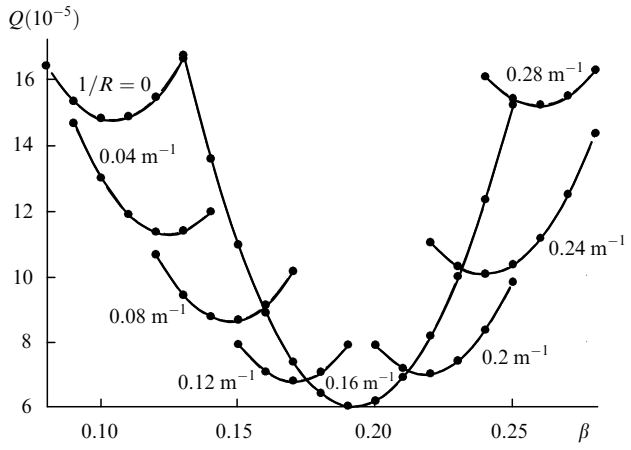

Figure 6. Dependences of the optimisation parameter Q on β for different parameters $1/R$.

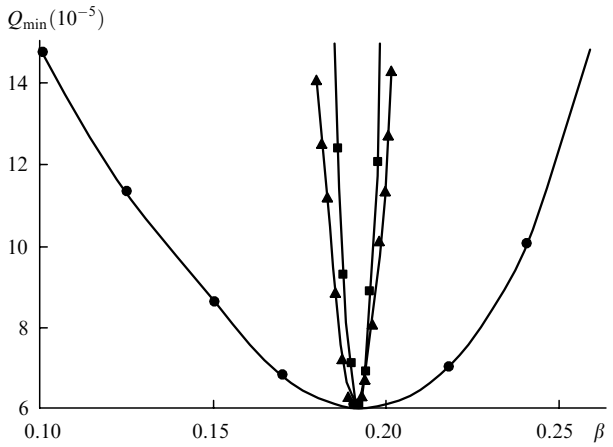

Figure 7. Dependences of the minimal optimisation parameter $Q_{\min}$ on the optimal values of β obtained by varying parameters R(●), Λ (▲), and I_s (■).

The interferometric control of the wave-front planeness in experiments with a free-running laser is complicated due to a small coherence length of radiation. However, using the obtained intensity distributions in the probe beam, we can determine independently the radius R of curvature of the wave front by measuring the average distance between the maxima Λ_i (minima) of the interference pattern during the propagation of probe radiation along the z axis near the image of active element (*7*). It is easy to verify that $R = \Lambda_i(\mathrm{d}\Lambda_i/\mathrm{d}z)^{-1}$.

The radii of curvature determined by this method coincided within the experimental error of $\pm 10\,\%$ with the values calculated from the contrast-variation curves. Unlike R, variations in the parameter Λ, and I_s do not lead to substantial changes in the optimal values of the parameter β found by the method of least squares. Because these parameters can be quite accurately determined from the contrast-variation curve, the error of their calculation almost does not affect the accuracy of measurement of β.

Since the calculations were performed in the approximation of a 'thin' amplifying medium, the systematic error in the determination of the parameter β was introduced by a finite length of active element (*7*). To minimise this error, the central region of the image of active element (*7*) located at equal distances from the images of its ends was taken as the origin of the longitudinal coordinate z. In this case, the uncertainty in the calculation of the coordinate z was half the reduced length of active element (*7*) [$(L/(2n) = 1.6$ cm]. For the grating step $\Lambda = 1$ mm, this introduced an additional error in the calculation of the parameter β equal to ± 0.06. Note that this error can be easily eliminated in a more accurate mathematical model taking into account the interaction of waves on the gain grating in the active medium.

Considering the accuracy of measuring the parameter β, one should bear in mind that, aside from random errors in the determination of the contrast of the transverse distribution of probe radiation, there also exist systematic errors caused by wave-front aberrations and the inhomogeneity of the transverse intensity distribution of the probe beam, the imperfection of a mathematical model used, and by other factors. All these errors can contribute to the discrepancy between experimental and calculated data characterised by $Q_{\min}$.

To improve the reliability of the results, we will assume that the errors of this method corresponds to the region of β where the optimisation parameter Q can take values lower than $(2+1/\sqrt{N})Q_{\min}$. Thus, if the gain saturation is low (Fig. 6), the parameter β, taking into account the error in the measurement of the coordinate z, can be estimated as 0.19 ± 0.15 when the parameter R is unknown and as 0.19 ± 0.11 when R was calculated independently. In our experiments with the energy of saturating beams equal to 16 mJ (see Fig. 5a), the parameter β, found by varying simultaneously β and R, was 0.14 ± 0.16.

5. Discussion of results

The results of this paper confirm the existence of the phase component of the saturated gain grating in a flashlamp-pumped Nd : YAG crystal. At the same time, we did not reveal a substantial increase in the parameter β in the region of high gains ($\alpha > 0.3$ cm^{-1}) observed in Refs [12, 17]. This discrepancy can be explained by the specificity of our experimental conditions. In particular, we used the 0.2 % aqueous solution of potassium dichromate ($K_2Cr_2O_7$) as a coolant. This solution is employed in cooling systems of solid-state lasers to prevent the radiative colouring of laser crystals caused by the short-wavelength pump radiation. According to Ref. [22], a 3-mm layer of the 2 % solution of potassium dichromate (~ 0.7 % of the normal concentration or 2 g L^{-1}) strongly absorbs pump radiation at wavelength shorter than 430 nm, preventing the population of the $^2(F_2)_{5/2}$ level of the Nd^{3+} ion directly from the metastable $^4F_{3/2}$ level. It seems that the population of other metastable levels ($^4D_{3/2}$, and $^2P_{3/2}$) of the 4*f* shell affects the polarisability of the active medium at the lasing frequency to a lesser degree because these energy levels are far removed from the levels of the 5*d* shell.

6. Conclusions

In this paper, we have proposed the method for direct measurements of the ratio of the amplitude and phase components of the gain grating. The use of the Talbot effect allows us to abandon the employment of probe beams at the nonresonance frequency for separating the phase component of the grating, which improves the reliability of measurements of the ratio of the real and imaginary parts of the resonance susceptibility of a laser medium. Our study showed that the ratio of the real and imaginary parts of the resonance susceptibility of flashlamp-pumped a Nd : YAG laser crystal measured when the short-wavelength pump radiation was rejected did not exceed 0.3 for the gain $\alpha < 0.5$ cm^{-1}.

Acknowledgements. This work was supported by the Russian Foundation for Basic Research (Grant No. 03-02-17316) and INTAS (Grant No. 03-51-4893).

References

1. Brignon A., Loiseau L., Larat C., Huignard J.-P., Pocholle J.-P. *Appl. Phys. B*, **69**, 159 (1999).
2. Afanas'ev L.A., Ionin A.A., Kiselev E.A., Klimachev Yu.N., Kotkov A.A., Sinitsyn D.V. *Kvantovaya Elektron.*, **21**, 557 (1994) [*Quantum Electron.*, **24**, 513 (1994)].
3. Antipov O.L., Belyaev S.I., Kuzhelev A.S. *Opt. Commun.*, **117**, 290 (1995).
4. Brignon A., Huignard J.-P. *Opt. Commun.*, **119**, 171 (1995).
5. Bel'dyugin I.M., Zolotarev M.V., Kireev S.E., Odintsov A.I. *Kvantovaya Elektron.*, **13**, 825 (1986) [*Sov. J. Quantum Electron.*, **16**, 535 (1986)].
6. Bel'dyugin I.M., Berenberg V.A., Vasil'ev A.E., Mochalov I.V., Petnikova V.M., Petrovskii G.T., Kharchenko M.A., Shuvalov V.V. *Kvantovaya Elektron.*, **16**, 1142 (1989) [*Sov. J. Quantum Electron.*, **19**, 740 (1989)].
7. Damzen M.J., Green R.P.M., Syed K.S. *Opt. Lett.*, **20**, 1704 (1995).
8. Denisov A.A., Kulikov O.L., Pilipetskii N.F. *Kvantovaya Elektron.*, **16**, 658 (1989) [*Sov. J. Quantum Electron.*, **19**, 429 (1989)].
9. Pashinin P.P., Sidorin V.S., Tumorin V.V., Shklovskii E.I. *Kvantovaya Elektron.*, **24**, 55 (1997) [*Quantum Electron.*, **27**, 52 (1997)].
10. Pashinin P.P., Tumorin V.V., Shklovskii E.I. *Kvantovaya Elektron.*, **25**, 727 (1998) [*Quantum Electron.*, **28**, 707 (1998)].
11. Antipov O.L., Kuzhelev A.S., Chausov D.V. *Opt. Express*, **5** (12), 286 (1999).
12. Antipov O.L., Kuzhelev A.S., Chausov D.V. *Izv. Ross. Akad. Nauk. Ser. Fiz.*, **63**, 740 (1999).
13. Galushkin M.G., Mitin K.V., Sviridov K.A. *Kvantovaya Elektron.*, **21**, 1157 (1994) [*Quantum Electron.*, **24**, 1073 (1994)].
14. Zverev G.M., Golyaev Yu.D., Shalaev E.A., Shokin A.A. *Lazery na alyumoittrievom granate s neodimom* (Nd : YAG Lasers) (Moscow: Radio I Svyaz', 1985).
15. Voronin V.G., Nanii O.E., Pankratov A.V. *Kvantovaya Elektron.*, **29**, 106 (1999) [*Quantum Electron.*, **29**, 944 (1999)].
16. Polushkin N.I., Khandokhin P.A., Khanin Ya.I. *Kvantovaya Elektron.*, **10**, 1461 (1983) [*Sov. J. Quantum Electron.*, **13**, 950 (1983)].
17. Antipov O.L., Kuzhelev A.S., Luk'yanov A.Yu., Zinov'ev A.P. *Kvantovaya Elektron.*, **25**, 891 (1998) [*Quantum Electron.*, **28**, 867 (1998)].
18. Antipov O.L., Chausov D.V., Yarovoy V.V. *Opt. Commun.*, **189**, 143 (2001).
19. Bufetova G.A., Nikolaev D.A., Shcherbakov I.A., Tsvetkov V.B. *Laser Phys.*, **13**, 245 (2003).
20. Patorski K. *Progress in Optics*, **27**, 3 (1989).
21. Woerdman J.P. *Phys. Lett.*, **32A**, 305 (1970).
22. Jones H.C., Strong W.W. *A Study of the Absorption Spectra* (Washington, D.C.: Carnegie Institution of Washington, 1910) p. 26.